

Synthesis and characterization of calcium phosphate coatings on Nitinol

Jozefina Katić · Mirjana Metikoš-Huković · Ranko Babić

Received: 19 June 2013 / Accepted: 3 August 2013 / Published online: 18 August 2013
© Springer Science+Business Media Dordrecht 2013

Abstract In recent years, coating of metal orthopedic implants with bioactive layers to promote fixation with bones has become increasingly common. Calcium phosphate coatings on the Nitinol surface were formed using two low-temperature methods: sol–gel and electrochemically assisted deposition. The coatings formed were characterized using: X-ray diffraction analysis, field emission scanning electron microscopy, energy dispersive X-ray spectroscopy, and Fourier transform infrared spectroscopy. Cyclic voltammetry studies were carried out in the deposition solution to determine parameters for electrodeposition and to understand electrochemistry of deposition. The barrier properties and corrosion resistance of coatings were tested in the physiological Hanks' solution using electrochemical impedance spectroscopy. The sol–gel deposited coating consisted of two phases, hydroxyapatite and tricalcium phosphate (TCP). Apatite coatings containing TCP offered the opportunity to create a grafting material with high bioactivity and bioresorbility. The electrodeposited coating consisted of Ca-deficient HAp which resembles to biological HAp.

Keywords Electrodeposition · Sol–gel method · Nitinol · Biphasic calcium phosphate · Ca-deficient hydroxyapatite · Surface modification

1 Introduction

Due to their bioactivity and biocompatibility with bone tissues, calcium phosphates (CaP) have been in use in medicine and dentistry for the last 30 years (grafts for bone growth, bone fillers, coatings on orthopedic and dental implants, in maxillofacial surgery and otolaryngology) [1–3]. Particularly attractive is hydroxyapatite [$\text{Ca}_{10}(\text{PO}_4)_6(\text{OH})_2$, HAp], a major inorganic component of natural bone [4]. HAp is recognized as osteoconductive, able to accelerate bone ingrowth and attachment to the surface of implant during the early stage after implantation, and to improve the fixation and lifetime of the implant [1, 3]. Nevertheless, poor mechanical properties limit its use to no load-bearing conditions [3]. These drawbacks can be overcome by using the CaP coatings on the high-strength metals/alloys such as titanium and titanium alloys.

Nitinol, the titanium–nickel alloy, has been widely used in the field of dentistry and orthopedic surgery owing to its unique properties, such as shape memory effect, superelasticity, and high damping capacity [5]. Although Nitinol possesses high corrosion resistance in physiological solutions caused by the spontaneously formed passive film of TiO_2 [5, 6], the major concern regarding its biocompatibility is release of allergenic and toxic Ni^{2+} ions due to in vivo corrosion. To prevent nickel dissolution, Nitinol has been modified using different surface treatments [7, 8]. In fact, as the other metallic materials, Nitinol and Ti-based alloys are classified as bioinert materials as they do not induce bone formation on their surface [9]. Hence, metallic implants with CaP coatings offer the combined advantages of the excellent mechanical properties of the metal and remarkable biocompatibility of the CaP ceramics, enabling the load-bearing implant applications and encouraging the bone tissue ingrowth, attachment of cells, and their subsequent multiplication [10].

J. Katić · M. Metikoš-Huković (✉) · R. Babić
Department of Electrochemistry, Faculty of Chemical
Engineering and Technology, University of Zagreb, Savska c.
16, P.O. Box 177, 10000 Zagreb, Croatia
e-mail: mmetik@fkit.hr

Different methods are used for the formation of CaP/HAp coatings on titanium/titanium alloys: electrocrystallization, biomimetic processes, plasma or thermal spraying, polymeric route, electrophoretic deposition, sputtering, etc. [11, 12]; with plasma spraying being the most common and commercialized method. Albeit, these methods were successful in HAp coatings formation, they have severe limitations: complicated preparation procedures, high temperature treatments which deteriorate the metal substrates, unnecessary phases besides HAp formed in the coatings, poor adhesion, lack of uniformity of coatings in terms of both morphology and crystallinity, delamination leading to premature wear, and loosening of the implants and sophisticated equipment required [13–15].

The sol–gel method and electrochemically assisted deposition, two of the most promising processes, have gained more attention due to their advantages in comparison to other conventional methods [13, 16–18]. Much interest in electrodeposition has evolved due to the low temperatures involved, which enable formation of highly crystalline deposits with low solubility in body fluids and low residual stresses [19], the ability to coat porous, geometrically complex surfaces, the ability to control the thickness, composition, and microstructure of the deposit, the possible improvement of the substrate/coating bond strength, and low cost of equipment [18, 20, 21]. The most attractive characteristics of sol–gel method are: higher homogeneity at molecular level (easily achieved by mixing the two solutions), easy control of chemical composition (better purity; ratio of mixed solutions is maintained in the final product), relatively low-temperature synthesis [12, 22]. The calcination process was used to densify the layer (residual organics decompose, decrease the porosity) and improve its adhesion towards the substrate [13, 23]. Low calcining temperatures can lead to weakly bonded low density coatings, but high calcining temperatures result in degradation of metal substrate catalyzing the decomposition of HAp [24]. It was shown previously that a temperature between 375 and 450 °C was required to develop CaP phase for the coating on metal substrates [25, 26]. At temperatures higher than 1,200 °C, HAp decomposes into tricalcium phosphate (TCP) and tetracalcium phosphate [27]. On the other hand, at temperature above 750 °C predominant TiO₂ rutile phase reacts with CaP layer forming CaTiO₃ intermediate [27]. In this paper, the moderate temperature (450 °C) was chosen for calcination process to obtain CaP coating on the Nitinol surface produced by sol–gel dip-coating deposition method.

In the present work, the Nitinol surface was modified with CaP ceramic coatings using two low-temperature methods: sol–gel method and electrochemical deposition. Both of these protection methods combine good mechanical properties of the metallic substrate with good biocompatibility of CaP. The microstructure of CaP coatings was characterized

by field emission scanning electron microscopy (SEM). The chemical composition was examined using energy dispersive X-ray spectroscopy (EDS), X-ray diffraction analysis (XRD), and Fourier transform infrared spectroscopy (FTIR). The barrier properties of coatings were tested in the physiological Hanks' solution using electrochemical impedance spectroscopy (EIS).

2 Experimental

The Nitinol foil (with the wt% content of: 55.82 Ni, ≤ 0.05 C, ≤ 0.05 O, ≤ 0.20 other metal impurities, and balance Ti) was cut into 0.38-mm-thick disks with 13 mm diameter. Circular-shaped Nitinol electrodes were polished with SiC papers of 240–1,200 grit, and ultrasonically cleaned with acetone and redistilled water.

2.1 Coating methods

2.1.1 Sol–gel deposition method

Sol–gel synthesis/preparation: 10 g of calcium 2-ethylhexanoate (Ca(EHA)₂; 98 wt%, Aldrich) was dissolved in 28.6 mL of ethylhexanoic acid (EHA; 99 wt%, Aldrich). To produce the sol of CaP with Ca/P molar ratio of 1.67, the above solution was mixed with 4.76 mL of 2-ethylhexyl-phosphate (EHP; 95 wt%, Merck, mixture of 45 % mono- and 55 % di-ester of phosphoric acid). After adding ethanol to reduce the overall CaP concentration to 5 wt%, the sol was stirred at 21 ± 2 °C for 4 h before being used for coating. The sol was dried at 130 °C for 4 h and the resulting yellow sticky gel was calcined at 450 and 600 °C for further characterization. The freshly prepared Nitinol samples were kept at 90 °C for 30 min in a regular air-convection oven. The coating was performed by dipping the samples into the CaP sol at 21 ± 2 °C, pulling them out at a speed of approximately 6 cm min⁻¹, drying in air at 130 °C for 4 h, and calcining in a preheated furnace at 600 °C for 10 min. The multilayered coatings on Nitinol were prepared by cycling the above procedure.

2.1.2 Electrochemically assisted deposition method

Nitinol samples, prepared as described previously, were treated in 1 M NaOH for 1 h at 80 °C prior to coating. The electrodeposition was performed in aqueous solution consisting of mixture of 0.1 mol dm⁻³ Ca(NO₃)₂ and 0.06 mol dm⁻³ NH₄H₂PO₄. The electrodeposition was carried out potentiostatically at -1.15 V for 2 h. To maintain the Ca²⁺ and H₂PO₄²⁻ concentration uniform during the electrodeposition, the solution was mixed using magnetic mixer. After coating, the Nitinol samples were

post-treated in the 1 M NaOH solution for 1 h at 80 °C and subsequently rinsed in redistilled water.

Cyclic voltammetry (CV) measurements (in the potential range from -1.5 to 1.5 V, scan rate of 10 mV s^{-1}) were performed in the deposition electrolyte to investigate the electrodeposition of CaP on Nitinol and determine conditions of electrodeposition. The kinetic parameters of this process were identified based on the CV criteria from cyclic voltammograms recorded on Nitinol in the deposition electrolyte at different scan rates, $v = 10\text{--}120 \text{ mV s}^{-1}$.

2.2 Methods for coatings characterization

Phase analysis of CaP gel obtained was accomplished by XRD. The XRD patterns were recorded at 20 ± 2 °C using APD 2,000 X-ray powder diffractometer (Cu K α radiation, 2θ step of $0.02^\circ/10$ s, graphite monochromator, NaI-Tl detector) manufactured by *ItalStructures*, Riva Del Garda, Italy.

The microstructure and morphology of the coatings on the Nitinol substrates were determined by field emission SEM using Jeol Ltd. FE SEM, model JSM-7000F. An elemental analysis was performed by EDS using Oxford Instruments Ltd. EDS/INCA 350 in addition to SEM.

The FTIR spectra were recorded in the $4,000\text{--}650 \text{ cm}^{-1}$ region using horizontal attenuated total reflectance (HATR) method on a Perkin-Elmer Spectrum One FTIR spectrometer.

For the impedance spectroscopy measurements (EIS) a three-electrode cell (PAR, Corrosion cell system, model K47) was used. The counter electrode consisted of two graphite rods and the reference electrode, to which all potentials in the paper are referred, was an Ag | AgCl, 3.0 mol dm^{-3} KCl ($E = 0.208$ V vs. standard hydrogen electrode). The surface area of working electrodes exposed to the electrolyte was 1 cm^2 . The corrosion behavior of coated and uncoated Nitinol was studied in the Hanks' solution at 37 °C performed at E_{OCP} in the frequency range from 10^5 to 10^{-3} Hz with an *ac* voltage amplitude of ± 5 mV using a Solartron frequency response analyzer SI 1,255 and Solartron electrochemical interface 1,287. Impedance measurements were performed after 1 h of stabilization at E_{OCP} . The experimental data were fitted using the complex non-linear least squares (CNLS) fit analysis [28] software ZView[®], and values of the elements of the proposed equivalent circuit were derived with χ^2 values less than 2×10^{-3} and relative error values below 5 %.

3 Results and discussion

3.1 Sol–gel synthesized CaP coatings on Nitinol

The phases formed in the synthesized and calcined sol were investigated using XRD analysis, powerful tool to

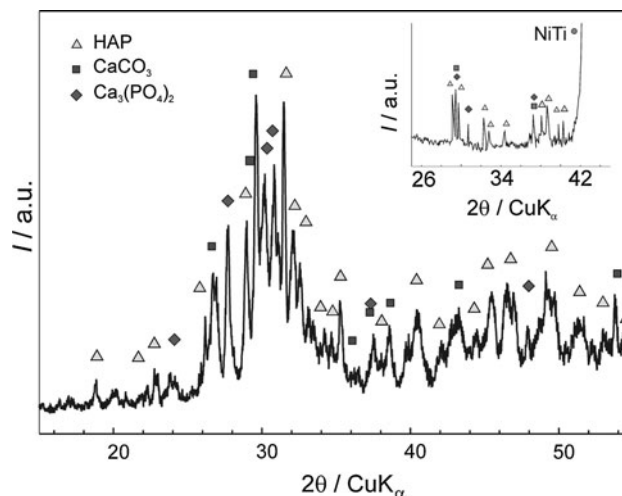


Fig. 1 The XRD pattern for the gel and the coating (*inset*) obtained by sol–gel process

determine the phase composition and crystallinity of the structure. Figure 1 presents the XRD pattern for the powder calcined at 600 °C.

Identification of the phases was performed by comparing the experimental XRD patterns to standards compiled by the Joint Committee on Powder Diffraction Standards (JCPDS) [29] using the cards no. 09-0432 for HAP, 29-0359 for TCP, and 85-1108 for calcite. By comparison with reference data, the XRD measurements indicate that the sol–gel powder shows the crystalline structure of HAP, TCP, and calcite mixture. A broad reflection peak in the range of $31.8\text{--}32.5^\circ$ of 2θ values corresponds to the apatite phase. The carbonate content, incorporated into crystal structure as calcite, is result of organic matter burn-off (precursors' pyrolysis) during gel calcination [30].

The XRD analysis of CaP coatings deposited on Nitinol was also performed (*inset* in Fig. 1). Although the weak XRD patterns were observed, still distinguishable signals appear, representing the presence of some phases in coatings as in the powder sample. The sol–gel method proposed resulted in formation of HAP, TCP, and calcite mixture, i.e., successful formation of CaP coatings on the Nitinol surface.

The microstructure and morphological characteristics of the CaP coatings on Nitinol were characterized by SEM and the composition was examined using EDS. Figure 2 presents SEM images of Nitinol substrate coated by 10 CaP layers.

Figure 2 shows that the multi-layered CaP coatings consisted of island like structures/flat surfaces with pores/cracks in between. In the pores/cracks the CaP bone-like nanometer structure was observed. In contrast, the single-layer coatings showed the presence of Ti and Ni signals in the pores/cracks [31]; indicating that the Nitinol substrate was in the direct

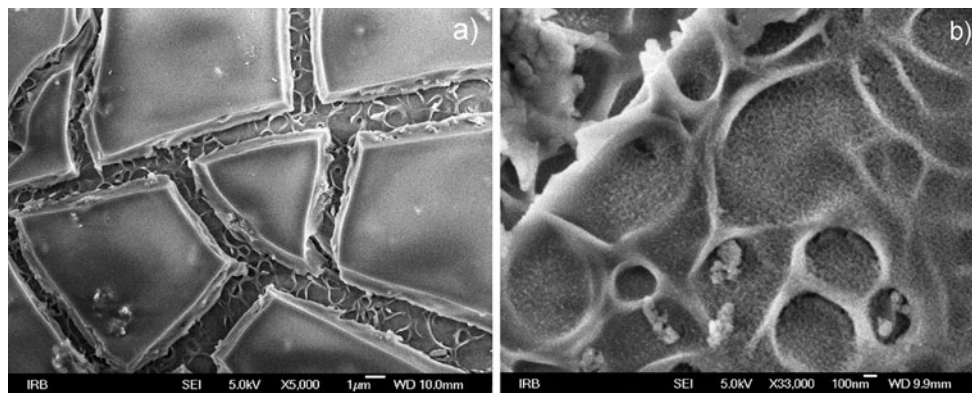


Fig. 2 SEM images of Nitinol substrates coated by 10 CaP layers

contact with aggressive body fluids. The cracked upper-layer CaP structure was indicative of coatings high shrinkage [32]. The formation of cracks in the upper CaP layers occurs due to densification and thermal stresses originated from the mismatch between thermal expansions coefficients of metallic substrate ($\alpha_{Ti} = 8.7 \times 10^{-6}/K$) and CaP coating ($\alpha_{HAp} = 13.6 \times 10^{-6}/K$) [33]. Since the thermal expansion coefficient of the coating is higher than for the substrate, it results in residual tensile stresses in the coating [32]. The presence of TiO_2 on NiTi substrate, with relatively lower thermal expansion coefficient ($\alpha_{TiO_2} = 7.249 \times 10^{-6}/K$) leads to a thermal expansion mismatch reduction between HAp and Ti alloy [9].

Multi-layered CaP coating strategy was successful in overcoming of the crack structure formation during densification. Added upper CaP coatings filled in the pores/cracks of cracked lower CaP coatings resulting in crack-healing of lower layers and formation of indented bone-like structure that also serves as a good base for bonding upper layers (Fig. 2b) [32]. The presence of porosity in this CaP coating is advantageous as it presumably enhances the osseointegration [34]. It should be taken into account that the OH^- and PO_4^{3-} ions on coating surfaces can combine with the Ca^{2+} ions in the body fluids to induce the formation of the bone-like apatite [35]. Therefore, good bioactivity can be imparted to Nitinol via CaP coatings.

The EDS analysis confirmed the formation coating with Ca/P molar ratio of 1.57, the mixture of HAp and TCP that corroborated the XRD results. The EDS analysis performed on multi-layered CaP coatings does not show any trace of Ti or Ni signals on the overall surface confirming the complete coverage of the substrate.

In addition, the sol-gel synthesized biphasic CaP ceramic coatings show an optimum balance of the most stable phase of HAp and more soluble TCP phase. Low content of TCP in bioceramic material is helpful for the enhanced osseointegration; i.e., rapid bonding the artificial bones/implants to natural ones via rapid CaP dissolution

[15, 36, 37]. It should be also noted, that the presence of CaP in the coating mimics the bone composition and gives an added advantage because it leads to enhanced osseointegration [9]. Thus, the sol-gel method offers the opportunity to create grafting material with excellent bioactivity, resorbability, and biocompatibility.

Electrochemical (corrosion) behavior as well as dielectric and electric properties of the NiTi | CaP interfaces in a simulated physiological solution at 37 °C were investigated using EIS. Measurements were performed at E_{OCP} over the wide frequency range. Impedance spectra of Nitinol samples coated with multilayered CaP in the form of Nyquist plot show response almost parallel to the axis of the impedance imaginary part and in the form of Bode plot exhibit capacitance behavior inside a broad frequency region in which the slope of the $\log |Z|$ against $\log f$ straight lines is close to -1 and high phase angle values (Fig. 3a). These characteristics point to the behavior typical for blocked (insulated) electrodes.

The corresponding electric equivalent circuit (EEC) for the blocking electrode consists of a constant phase element, CPE in series with an ohmic resistance, R_Ω . Because the measured capacitive response is not generally ideal due to certain heterogeneity of the electrode surface [38], a CPE has been introduced for fitting the spectra, instead of an ideal capacitance element, C . Its impedance can be defined by $Z(CPE) = [Q(j\omega)^n]^{-1}$, where Q is a constant, ω is the angular frequency, and n is the CPE power [39]. The factor n is an adjustable parameter, which has values between -1 and 1 . For the value of $n \geq ca. 0.9$, the capacitance values were calculated using the expression given by Brug et al. [40]:

$$C = (QR_\Omega^{1-n})^{\frac{1}{n}} \quad (1)$$

The EIS parameter values are listed in Table 1. The numerical values of interfacial capacitance, C were calculated using the Brug's expression, Eq. (1).

The justification for the application of a blocking circuit in representing the EIS data for multilayered CaP coatings

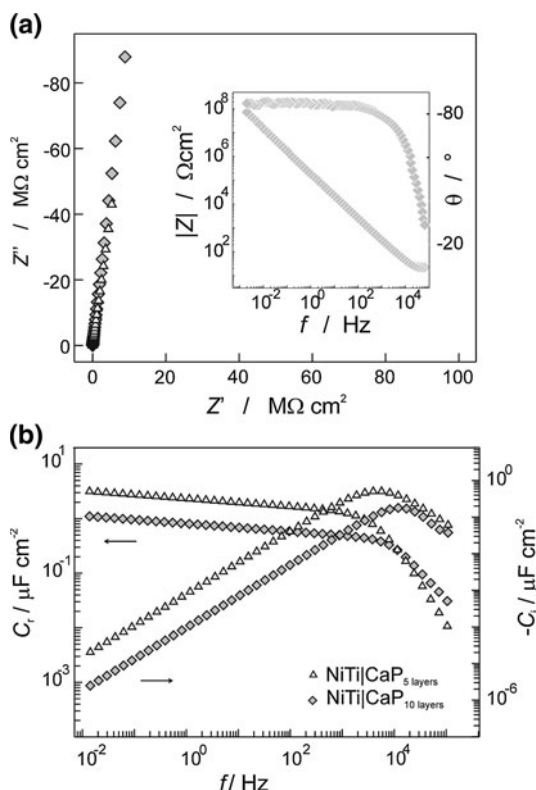


Fig. 3 Nyquist and Bode (*inset*) plots (a) and real and imaginary parts of the complex capacitance on a logarithmic scale as a function of frequency (b) for the impedance data of CaP coated (5 and 10 layers) Nitinol electrodes recorded in Hanks’ solution (37 °C) at E_{OCP}

was tested on the basis of the dependence of real, C_r and imaginary, C_j parts of the complex capacitance on a logarithmic scale as a function of frequency (see Fig. 3b) [41]. The complex-capacitance representation of EIS data is often used for solid-state and dielectric systems for which the complex capacitance is defined as [41]:

$$C(\omega) = C_r + jC_j = \frac{C}{1 + (\omega R_\Omega C)^2} - j \frac{R_\Omega \omega (C)^2}{1 + (\omega R_\Omega C)^2} \quad (2)$$

The characteristic frequency, f_c evident as a peak for the imaginary part of the complex capacitance (Fig. 3b) has a value corresponding to:

$$f_c = (2\pi R_\Omega C)^{-1} \quad (3)$$

and provides a direct determination of the interfacial capacitance, C whose values are listed in Table 1. As can

be seen from Table 1 capacitance values determined from EEC modeling and from characteristic frequencies are almost the same and confirm the presentation of multilayered CaP coatings as the blocking system. The resistance of the CaP surface layer $R \rightarrow \infty$, and dc corrosion current $\rightarrow 0$, which means, the prevention of a flow of charged/solvated ions towards the NiTi surface and/or dissolution of Ti and Ni ions in the solution.

From Table 1 and Fig. 3 it is clearly visible that by increasing the number of CaP coatings, capacitance values decrease. The structure of the multilayered CaP coating is compact and homogeneous and acts as the blocking contact, which prevents charge-transfer reactions of the NiTi surface in a physiological solution. Excluding other biocompatibility-governing factors, these surfaces would be, from the corrosion stability point of view, good candidates for biocompatible surfaces.

3.2 “Electrochemically” deposited CaP coatings on Nitinol

Besides the sol–gel method, the CaP coatings were deposited on Nitinol using the electrochemically assisted method. Formation of HAP coatings was obtained by the two step procedure: electrochemical and chemical. Cyclic voltammetry investigations were carried out in the deposition solution to determine parameters for electrodeposition and to understand chemistry of CaP coating deposition on metallic substrates (implants). Figure 4 presents cyclic voltammogram recorded in the potential range from potential of hydrogen evolution to potential of oxygen evolution.

Anodic part of the voltammogram shows current density values independent on potential, up to beginning of the oxygen evolution process, pointing to formation of surface film during linear polarization. In backward part of voltammogram the characteristic nucleation loop [42] at -0.57 V (see the inset in Fig. 4) as well as the characteristic sharp reduction current peak at -1.15 V are connected with the formation of a new solid phase on the Nitinol surface.

The cathodic reaction is electrochemical deprotonation of hydrogen from $H_2PO_4^-$ ions

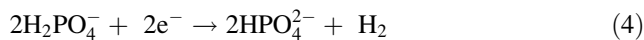
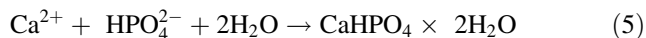


Table 1 Impedance parameters of Nitinol samples coated with multilayered CaP coatings, obtained in Hanks’ solution (37 °C) at E_{OCP}

Samples	$10^6 \times Q_1/\Omega^{-1} \text{ cm}^{-2} \text{ s}^n$	n_1	$C_{Brugg}/\mu\text{F cm}^{-2}$	f_c/kHz	$C/\mu\text{F cm}^{-2}$
NiTi CaP _{5 layers}	2.62	0.93	1.26	5.01	1.27
NiTi CaP _{10 layers}	0.92	0.93	0.40	12.59	0.40

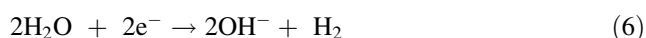
$$R_\Omega = 21 \pm 5 \Omega \text{ cm}^2$$

It is expected that HPO_4^{2-} ions produced completely or partially react with Ca^{2+} ions and form insoluble coating on the electrode surface (brushite, $\text{CaHPO}_4 \times 2\text{H}_2\text{O}$) according to following reaction:



The observed current density values of the cathodic peak are around 1 mA cm^{-2} , see Fig. 4. It was shown that electrodeposition at current densities around 1 mA cm^{-2} , resulted in formation of brushite on metallic implant materials at the interfacial pH lower than 6.7, because concentration of OH^- ions is insufficient to convert all HPO_4^{2-} into PO_4^{3-} according to the acid–base reaction: $\text{HPO}_4^{2-} + \text{OH}^- \rightarrow \text{PO}_4^{3-} + \text{H}_2\text{O}$ [43, 44].

At higher cathodic potentials ($E < -1.5 \text{ V}$), reduction of water becomes a dominant cathodic reaction (Fig. 4).



This cathodic reaction causes an increase in pH of a solution and enables neutralization of H_2PO_4^- .

To characterize the electrochemical process taking place on Nitinol in the deposition electrolyte in more detail, the influence of the scan rate on the cyclic voltammograms was investigated. The cyclic voltammograms were recorded on Nitinol in the potential range of brushite deposition at scan rates ranging from 10 to 120 mV s^{-1} (Fig. 5a).

The mechanism and kinetics of electrodeposition of brushite ($\text{CaHPO}_4 \times 2\text{H}_2\text{O}$) on Nitinol were analyzed on the basis of CV results (Fig. 5a) according to the diagnostic criteria of CV [45]. Figure 5b, including a corresponding insert, shows linear dependence of current density peak, j_p on the root-square of scan rate, $v^{1/2}$ and the linear dependence of $\log j_p$ on $\log v$ pointing that electrodeposition (electrocristallization) process occurs under diffusion control.

From a linear dependence of j_p on $v^{1/2}$, using the relation below, it is possible to determine values of diffusion coefficient, D [46]:

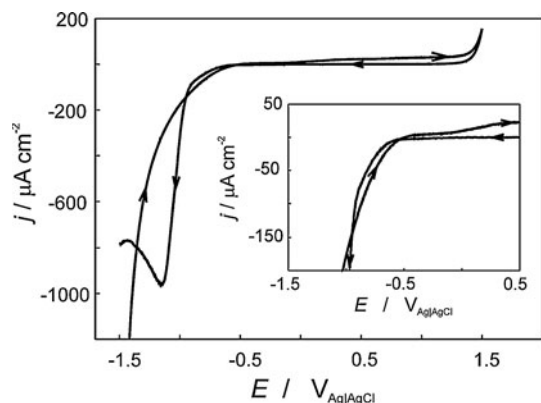


Fig. 4 Cyclic voltammogram of Nitinol recorded in the deposition electrolyte at scan rate, $v = 10 \text{ mV s}^{-1}$

$$j_p = -(2.99 \times 10^5 \text{ C mol}^{-1} \text{ V}^{-1/2}) z (\alpha_C z_\alpha)^{1/2} c_0^\infty D^{1/2} v^{1/2} \quad (7)$$

where c_0^∞ is the concentration of potential determining ions in the bulk of solution, α_C is the coefficient of transfer for cathodic process, z_α corresponds to the number of electrons transferred up to, and including, the rate determining step. The coefficient $\alpha_C z_\alpha$ is determined according to relation [45]:

$$|E_p - E_{p/2}| = \frac{48}{\alpha_C z_\alpha} \text{ mV} \quad (8)$$

where E_p is the potential of current peak, and $E_{p/2}$ is the potential at the half of the current density value peak, j_p . Numerical values of $\alpha_C z_\alpha$ and D are given in Table 2. The values obtained are in agreement to those reported in the literature [21].

Mean value of $D = 3.2 \times 10^{-6} \text{ cm}^2 \text{ s}^{-1}$ and the value of the thickness of the diffusion layer, $d = 0.01 \text{ cm}$ [21] enable to determine the current density of brushite deposition on Nitinol under diffusion control according to the relation of Fick's first law:

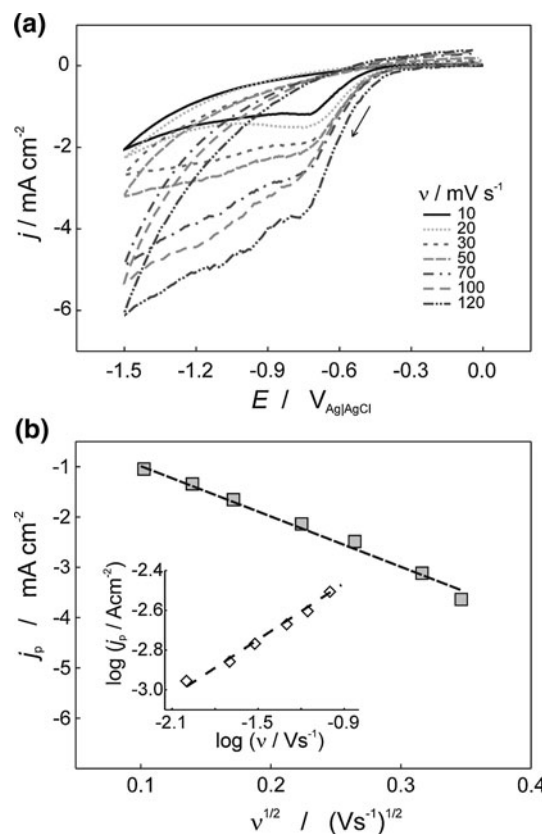


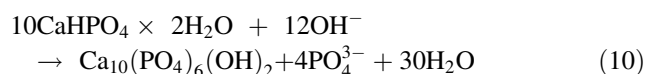
Fig. 5 **a** Cyclic voltammograms of Nitinol recorded in the deposition electrolyte in the potential range from 0 to -1.5 V at the scan rates noted. **b** Diagnostic criteria of cyclic voltammetry for the results presented in (a)

Table 2 Values of coefficients $\alpha_C z_\alpha$ and diffusion coefficients determined according to the cyclic voltammetry criteria

$v/\text{mV s}^{-1}$	$\alpha_C z_\alpha$	$D \times 10^6/\text{cm}^2 \text{ s}^{-1}$
120	0.318	3.916
100	0.348	3.579
70	0.384	3.243
50	0.397	3.137
30	0.400	3.113
20	0.421	2.958
10	0.471	2.644

$$j_L = zFDc/\delta \quad (9)$$

The determined current density of 1 mA cm^{-2} agrees with the experimentally examined value of the cathodic current peak, see CV in Fig. 4. The brushite coating, formed by the electrochemical step and deposition reactions (4–5), was subsequently alkali treated to obtain HAP [47, 48]:



Morphological characterization and chemical composition of CaP films on Nitinol were obtained by SEM/EDS. The analysis was performed on samples immediately after cathodic electrodeposition (Fig. 6a) and after the alkali treatment (Fig. 6b).

SEM images show formations of compact coatings with laminated structure. After alkali treatment, thicker laminated structure with surface particles can be observed. It should be also stressed out that no cracks/pores were present, visible for the sol–gel dip-coated Nitinol substrates (Fig. 2).

Chemical composition of CaP films formed by two steps procedure on Nitinol substrates were obtained by EDS. Results show formation of CaP coating with the Ca/P ratio of 1.01 [2, 49]; i.e., formation of calcium hydrogen phosphate dihydrate (brushite). The EDS results after the

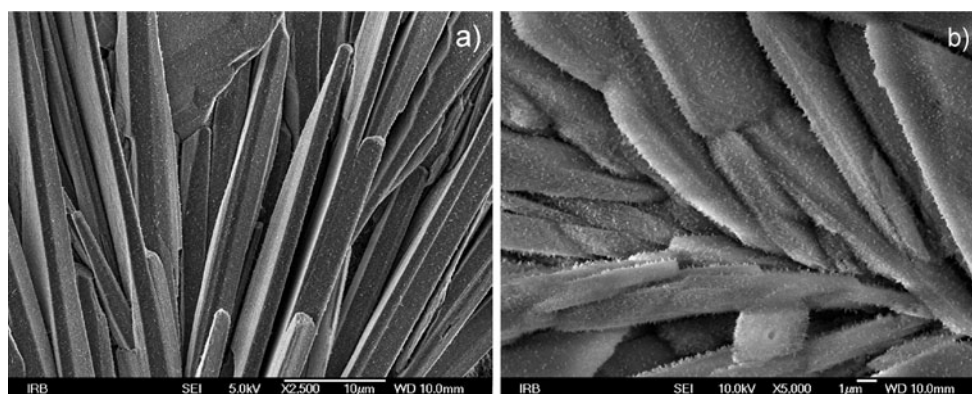
subsequent alkali treatment show the formation of CaP coating with the Ca/P ratio of 1.63, pointing to formation of Ca-deficient HAP [50, 51]. Brushite formed by electrodeposition serves as precursor for HAP.

The FTIR spectrum of Nitinol substrate coated by cathodically electrodeposited CaP film that was subsequently alkali treated is presented in Fig. 7. The prominent bands observed in the range of $900\text{--}1,200 \text{ cm}^{-1}$ are characteristic for phosphate groups present in the apatite structure [52]. The ν_1 P–O symmetric stretching vibrations and ν_3 asymmetric stretching vibrations were detected at around $1,020$, $1,130$, and $1,198 \text{ cm}^{-1}$, respectively [23, 53, 54]. Absorption bands present around $3,500$ and $2,850 \text{ cm}^{-1}$ are assigned to O–H stretch bands in HAP [53]. The latter band may be also due to the stretching vibration of P–O–H in distinct structural positions [55]. The band at $1,650 \text{ cm}^{-1}$ is associated to vibration modes of adsorbed water [23, 53].

Bands at 712 , 874 , $1,440$, and $1,734 \text{ cm}^{-1}$, characteristic of CO_3^{2-} species, are attributable to ν_4 , ν_2 , and ν_3 vibrational carbonate mode, respectively [52–54]. The observed bands resulted from the carbonate groups incorporated in the apatite structure and suggest B-type incorporation; i.e., CO_3^{2-} for PO_4^{3-} substitutions [56]. The carbonate comes from the atmosphere carbon dioxide which combined into the crystal structure during the coating preparation [57]. The carbonate content makes coating more similar to the natural bone mineral [58].

The corrosion behavior of HAP-uncoated (covered by spontaneously formed oxide film) and HAP-coated Nitinol samples (NiTi/HAP interface) prepared by electrochemically assisted deposition was examined in a simulated physiological solution (Hanks' solution, $37 \text{ }^\circ\text{C}$) by using a nondestructive method, EIS. Impedance spectra of uncoated and HAP coated Nitinol electrode, in the form of Nyquist and Bode plots, are presented in Fig. 8.

The impedance data were fitted using EEC model composed of an R - CPE parallel combination in series with an ohmic resistance R_{el} , where R is the polarization

**Fig. 6** SEM images of Nitinol coated with (a) brushite coating and (b) HAP coating

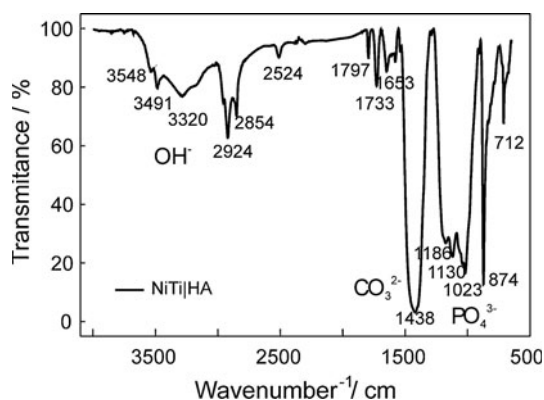


Fig. 7 FTIR spectrum of Nitinol coated with CaP deposited by the electrochemically assisted procedure

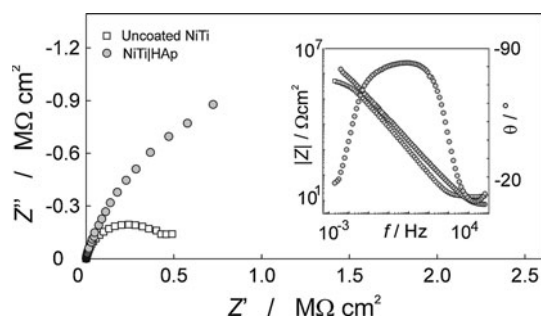


Fig. 8 The Nyquist and Bode (inset) plots of impedance spectra of uncoated and HAp-coated Nitinol electrodes recorded in a Hanks' solution (37 °C) at E_{ocp}

Table 3 Impedance parameters of uncoated and HAp-coated Nitinol electrodes, obtained in Hanks' solution (37 °C) at E_{ocp}

Samples	$10^6 \times Q_1 / \Omega^{-1} \text{ cm}^{-2} \text{ s}^n$	n_1	$C_{Brugg} / \mu\text{F cm}^{-2}$	$R / \text{M}\Omega \text{ cm}^2$
Uncoated NiTi	30.11	0.91	13.82	0.44
NiTi HAp	16.49	0.84	3.31	2.61

$$R_{\Omega} = 21 \pm 5 \Omega \text{ cm}^2$$

resistance R_p and CPE is used instead of ideal capacitance, C due to the frequency dispersion (mostly attributed to the “capacitance dispersion”) [38]. The interfacial capacitance, C was calculated using Eq. (1). Table 3 shows numerical values for the circuit parameters.

The protecting efficiency of the electrochemically deposited HAp film was calculated using the relation:

$$\eta = (R_{p,(\text{NiTi|HAp})} - R_{p,(\text{NiTi})}) / R_{p,(\text{NiTi|HAp})} \quad (11)$$

where $R_{p,(\text{NiTi|HAp})}$ and $R_{p,(\text{NiTi})}$ are the values of R_p in Table 3. The protecting efficiency of 83 % indicates good corrosion resistance of Nitinol coated with electrochemically deposited HAp film.

4 Conclusions

CaP coatings on the Nitinol surface were formed using two low-temperature methods: sol–gel and electrochemically assisted deposition. The sol–gel method offer the opportunity to form biphasic CaP coatings on metallic implants and to create a grafting material with high bioactivity and bioresorbility for medical applications. Electrochemically assisted method offer opportunity to form bioactive Ca-def. HAp deposits on the geometrically complex surfaces of metallic implants with low residual stresses and to control coatings morphology and chemical composition. The barrier properties and corrosion resistance of CaP coated Nitinol electrodes were tested in the Hanks' solution using EIS measurements. In the sol–gel procedure, thermal treatments caused the formation of the surface film of duplex structure (CaP coating beneath thermally formed TiO_2) that provide higher polarization resistance values (blocking interface) in comparison to the surface film formed by the electrochemically assisted procedure. In the later case, the protecting efficiency of 83 % indicate good corrosion resistance of HAp coated Nitinol substrates.

Acknowledgments The financial support of the Ministry of Science, Education and Sports of the Republic of Croatia under the 125-0982904-2923 Grant is gratefully acknowledged.

References

- Hench LL (1998) Bioceramics. *J Am Ceram Soc* 81:1705–1728
- Dorotzhkin S, Epple M (2002) Biological and medical significance of calcium phosphates. *Angew Chem Int Ed* 41:3131–3146
- Ratner BD, Hoffman AS, Schoen FJ, Lemons JE (eds) (2004) *Biomaterials science an introduction to materials in medicine*. Elsevier, San Diego
- Orlovski VP, Komlev VS, Barinov SM (2002) Hydroxyapatite and Hydroxyapatite-Based Ceramics. *Inorg Mater* 38:1159–1172
- Shabalovskaya SA (2002) Surface, corrosion and biocompatibility aspects of Nitinol as an implant material. *Bio-Med Mater Eng* 12:69–109
- Figuerira N, Silva TM, Carmezin MJ, Fernandes JCS (2009) Corrosion behaviour of NiTi alloy. *Electrochim Acta* 54:921–926
- Shabalovskaya SA, Anderegg J, van Humbeeck J (2008) Critical overview of Nitinol surfaces and their modifications for medical applications. *Acta Biomater* 4:447–467
- Liu X, Chu PK, Ding C (2004) Critical overview of Nitinol surfaces and their modifications for medical applications. *Mater Sci Eng R47*:49–121
- Mohan L, Durgalakshmi D, Geetha M, Sankara Narayanan TSN, Asokamani R (2012) Electrophoretic deposition of nanocomposite (HAp + TiO_2) on titanium alloy for biomedical applications. *Ceram Int* 38:3435–3443
- Dinda GP, Shin J, Mazumder J (2009) Pulsed laser deposition of hydroxyapatite thin films on Ti–6Al–4 V: effect of heat treatment on structure and properties. *Acta Biomater* 5:1821–1830
- Lewis G (2000) Hydroxyapatite-coated bioalloy surfaces: current status and future challenges. *Biomed Mater Eng* 10:157–188

12. Paital SR, Dahotre NB (2009) Calcium phosphate coatings for bio-implant applications: materials, performance factors, and methodologies. *Mater Sci Eng R* 66:1–70
13. Weng W, Baptista JL (1999) Preparation and characterization of hydroxyapatite coatings on Ti6Al4V alloy by a sol–gel method. *J Amer Ceram Soc* 82:27–32
14. Sun L, Berndt CC, Gross KA, Kucuk A (2001) Material fundamentals and clinical performance of plasma-sprayed hydroxyapatite coatings: a review. *J Biomed Mater Res B* 58:570–592
15. Ramanan SR, Venkatesh R (2004) A study of hydroxyapatite fibers prepared via sol–gel route. *Mater Lett* 58:3320–3323
16. Klein LC (1988) Sol–gel technology for thin films, fibers, preforms, electronics and specialty shapes. William Andrew Publishing, Noyes
17. Shirkanzadeh M (1998) Direct formation of nanophase hydroxyapatite on cathodically polarized electrodes. *J Mater Sci Mater Med* 9:67–72
18. Yang X, Zhang B, Lu J, Chen J, Zhang X, Gu Z (2010) Biomimetic Ca–P coating on pre-calcified Ti plates by electrodeposition method. *Appl Surf Sci* 256:2700–2704
19. Gopi D, Indira J, Kavitha L (2012) A comparative study on the direct and pulsed current electrodeposition of hydroxyapatite coatings on surgical grade stainless steel. *Surf Coat Technol* 260:2859–2869
20. Yen SK, Lin CM (2002) Cathodic reactions of electrolytic hydroxyapatite coating on pure titanium. *Mater Chem Phys* 77:70–76
21. Eliaz N, Elyahu M (2006) Electrochemical processes of nucleation and growth of hydroxyapatite on titanium supported by real-time electrochemical atomic force microscopy. *J Biomed Mater Res A* 80:621–634
22. Brinker CJ, Scherer GW (1992) Sol–gel science: the physics and chemistry of sol–gel processing. Academic Press, New York
23. Stoch A, Jastrzebski W, Dlugon E, Lejda W, Trybalska B, Stoch GJ, Adamczyk A (2005) Sol–gel derived hydroxyapatite coatings on titanium and its alloy Ti6Al4V. *J Molecul Struct* 744–747:633–640
24. Sridhar TM, Kamachi Mudali U, Subbaiyan M (2003) Sintering atmosphere and temperature effects on hydroxyapatite coated type 316L stainless steel. *Corr Sci* 45:2337–2359
25. Zhang JX, Guan RF, Zhang XP (2011) Synthesis and characterization of sol–gel hydroxyapatite coatings deposited on porous NiTi alloys. *J Alloys Compd* 509:4643–4648
26. Liu DM, Yang Q, Troczynski T (2002) Sol–gel hydroxyapatite coatings on stainless steel substrates. *Biomaterials* 23:691–698
27. Weng J, Liu X, Zhang X, Ji X (1994) Thermal decomposition of hydroxyapatite structure induced by titanium and its dioxide. *J Mater Sci Lett* 13:159–161
28. Boukamp A (1986) A nonlinear least squares fit procedure for analysis of immittance data of electrochemical systems. *Solid State Ionics* 20:31–44
29. International Centre for Diffraction Data, Joint Committee on Powder Diffraction Standards, Powder Diffraction File (1988), 1601 Park Lane, Swarthmore, PA 19081, USA
30. Gross KA, Chai CS, Kannagara GSK, Ben-Nissan B (1998) Thin hydroxyapatite coatings via sol–gel synthesis. *J Mater Sci: Mater Med* 9:839–843
31. Katić J, Metikoš-Huković M, Babić R, Marciuš M (2013) Sol–gel Derived Biphasic Calcium Phosphate Ceramics on Nitinol for Medical Applications. *Int J Electrochem Sci* 8:1394–1408
32. Wei M, Ruys AJ, Swain MV, Kim SH, Milthorpe BK, Sorrell CC (1999) Interfacial bond strength of electrophoretically deposited hydroxyapatite coatings on metals. *J Mater Sci: Mater Med* 10:401–409
33. Wang ZC, Ni YJ, Huang JC (2008) Fabrication and characterization of HAp/Al₂O₃ composite coating on titanium substrate. *Biomed Sci Eng* 1:190–194
34. Moskalewicz T, Czyrska-Filemonowicz A, Boccacini AR (2007) Microstructure of nanocrystalline TiO₂ films produced by electrophoretic deposition on Ti–6Al–7Nb alloy. *Surf Coating Technol* 201:7467–7471
35. Wen CE, Xu W, Hu WY, Hodgson PD (2007) Hydroxyapatite/titania sol–gel coatings on titanium–zirconium alloy for biomedical applications. *Acta Biomater* 3:403–410
36. Daculsi G (1998) Biphasic calcium phosphate concept applied to artificial bone, implant coating and injectable bone substitute. *Biomaterials* 19:1473–1478
37. Le Huec JC, Clement D, Brouillaud B, Barthe N, Dupuy B, Folliquet B, Basse-Cathalinat B (1998) Evolution of the local calcium content around irradiated β -tricalcium phosphate ceramic implants: in vivo study in the rabbit. *Biomaterials* 19:733–738
38. Lukacs Z (1999) Evaluation of model and dispersion parameters and their effects on the formation of constant-phase elements in equivalent circuits. *J Electroanal Chem* 464:68–75
39. Macdonald JR (1987) Impedance Spectroscopy: emphasizing solid materials and systems. John Wiley & Sons, New York, pp 27–98
40. Brug GJ, van der Eeden ALG, Sluyters-Rehbach M, Sluyters JH (1984) The analysis of electrode impedances complicated by the presence of a constant phase element. *J Electroanal Chem* 176:275–295
41. Orazem ME, Tribollet B (2008) Electrochemical impedance spectroscopy. John Wiley & Sons, Inc., Hoboken, pp 310–330
42. Arbib M, Zhang B, Lazarov V, Stoychev D, Milchev A, Buess-Herman C (2001) Electrochemical nucleation and growth of rhodium on gold substrates. *J Electroanal Chem* 510:67–77
43. Zhang JM, Lin CJ, Feng ZD, Tian ZW (1998) Mechanistic studies of electrodeposition for bioceramic coatings of calcium phosphates by an in situ pH-microsensor technique. *J Electroanal Chem* 452:235–240
44. Kuo MC, Yen SK (2002) The process of electrochemical deposited hydroxyapatite coatings on biomedical titanium at room temperature. *Mater Sci Eng C* 20:153–160
45. Southampton Electrochemistry Group (2001) Instrumental methods in electrochemistry. Horwood Publishing Limited, Eastborne, pp 178–189
46. Nicholson RS, Shain I (1964) Theory of stationary electrode polarography. Single scan and cyclic methods applied to reversible, irreversible, and kinetic systems. *Anal Chem* 36:706–723
47. Song Y, Zhang S, Li J, Zhao C, Zhang X (2010) Electrodeposition of Ca–P coatings on biodegradable Mg alloy: in vitro biomineralization behavior. *Acta Biomater* 6:1736–1742
48. Prado Da Silva MH, Lima JHC, Soares GA, Elias CN, de Andrade MC, Best SM, Gibson IR (2001) Transformation of monetite to hydroxyapatite in bioactive coatings on titanium. *Surf Coat Tech* 137:270–276
49. Vallet-Regi M, Gonzalez-Calbet JM (2004) Calcium phosphates as substitution of bone tissues. *Prog Solid State Chem* 32:1–31
50. Müller L, Müller FA (2006) Preparation of SBF with different HCO₃[−] content and its influence on the composition of biomimetic apatites. *Acta Biomater* 2:181–189
51. Dumelie N, Benhayoune H, Richard D, Laurent-Maquin D, Baloissier G (2008) In vitro precipitation of electrodeposited calcium-deficient hydroxyapatite coatings on Ti6Al4V substrate. *Mater Charact* 59:129–133
52. Rehman I, Bonfield W (1997) Characterization of hydroxyapatite and carbonated apatite by photo acoustic FTIR spectroscopy. *J Mater Sci Mater Med* 8:1–4
53. Popa MV, Moreno JMC, Popa M, Vasilescu E, Drob P, Vasilescu C, Drob SI (2011) Electrochemical deposition of bioactive coatings on Ti and Ti–6Al–4V surfaces. *Surf Coating Technol* 205:4776–4783
54. Koutsopoulos S (2002) Synthesis and characterization of hydroxyapatite crystals: a review study on the analytical methods. *J Biomed Mater Res* 62:600–612

55. Abo-Naf SM, El-Amiry MS, Abdel-Khalek AA (2008) FT-IR and UV-Vis optical absorption spectra of c-irradiated calcium phosphate glasses doped with Cr_2O_3 , V_2O_5 and Fe_2O_3 . *Opt Mater* 30:900–909
56. Layrolle P, Ito A, Tateishi T (1998) Sol-gel synthesis of amorphous calcium phosphate and sintering into microporous hydroxyapatite bioceramics. *J Am Ceram Soc* 81:1421–1428
57. Wang YJ, Chen JD, Wei K, Zhang SH, Wang XD (2006) Surfactant-assisted synthesis of hydroxyapatite particles. *Mater Lett* 60:3227–3231
58. Chen J, Wang Y, Chen X, Ren L, Lai C, He W, Zhang Q (2011) A simple sol-gel technique for synthesis of nanostructured hydroxyapatite, tricalcium phosphate and biphasic powders. *Mater Lett* 65:1923–1926